Acta Crystallographica Section B
Structural Science
ISSN 0108-7681

Incommensurately modulated lanthanide coinage-metal diarsenides. I. $CeAu_{1-\delta}As_2$ [δ = 0.015 (2)] – a new distortion variant of the $HfCuSi_2$ type with irregularly stacked *cis–trans* chains of arsenic atoms

D. Rutzinger, Th. Doert* and M. Ruck

Department of Chemistry and Food Chemistry, Technische Universität Dresden, D-01062 Dresden, Germany

Correspondence e-mail: thomas.doert@chemie.tu-dresden.de

Received 14 November 2008
Accepted 9 July 2009

Rare-earth metal coinage-metal diarsenides Ln*T*As$_2$ (Ln = Y, La, Ce–Lu; *T* = Cu, Ag, Au) are known to crystallize in structures closely related to the $HfCuSi_2$ type, which comprises a stacking sequence of puckered *T*As layers and planar square As nets, separated by the Ln atoms. $CeAu_{1-\delta}As_2$, with δ = 0.015 (2), shows an incommensurate positional modulation of the arsenic atoms in the planar As nets. Based on X-ray diffraction data on a twinned crystal, a structure model in the monoclinic superspace group $P12_1/m1(\alpha 0\gamma)00$ (No. 11.1) with basic unit-cell parameters of a = 5.804 (1), b = 5.814 (1), c = 10.179 (1) Å and β = 90.09 (8)° is presented. The components of the modulation wavevector $\mathbf{q} = \alpha\mathbf{a}^* + 0\mathbf{b}^* + \gamma\mathbf{c}^*$ are α = 0.08 (1) and γ = 0.39 (1). The structure comprises *cis–trans* chains and rectangles of As atoms and displays an intricate stacking sequence of the modulated arsenic nets. Rod groups and layer groups of the respective arrangements are identified and the arrangement of different motifs of the modulated As net is discussed.

1. Introduction

Compounds with layered-type structures are the subject of intensive investigations owing to both interesting structural features and physical properties. Among these, binary and ternary compounds of the compositions MT_4, MT_2X_2, MTX_2, $MT_{1\pm\delta}X_2$ and MX_2 have been investigated (M = alkaline, alkaline earth or rare-earth element, T = *d*-block element, X = element of group 13–15; Eisenmann *et al.*, 1970, 1972; Brechtel *et al.*, 1979; Zheng & Hoffmann, 1986; Venturini *et al.*, 1989*a*,*b*; Chykhrij *et al.*, 1997; Wang *et al.*, 1999). Numerous compounds of the general composition MTX_2 adopt the $HfCuSi_2$-type structure (Andrukhiv *et al.*, 1975; Sologub *et al.*, 1994; Brylak *et al.*, 1995; Sologub *et al.*, 1995; Wang *et al.*, 1999; Mozharivskiy *et al.*, 2000, 2001, 2002; Demchyna *et al.*, 2001; Kolenda *et al.*, 2001; Jemetio, Doert, Rademacher & Böttcher, 2002; Jemetio, Doert & Böttcher, 2002) or one of its distorted variants (Eschen & Jeitschko, 2003; Demchyna *et al.*, 2004). $HfCuSi_2$ crystallizes in the tetragonal space group $P4/nmm$ (No. 129; Andrukhiv *et al.*, 1975) with eight atoms in the unit cell. Characteristic features of the $HfCuSi_2$ structure are PbO-like layers formed by the Cu and Si1 atoms and planar square nets of the Si2 atoms. These motifs are separated by Hf atoms, which are embedded in the hollows of the CuSi layers (Fig. 1). In the ternary lanthanide compounds Ln*T*As$_2$ the lanthanide atoms Ln, the coinage metal atoms *T*, and the arsenic atoms occupy the Hf, Cu and Si positions, respectively.

Similar structural motifs have been found in the recently published iron-based layered superconductors LaFePO (Kamihara *et al.*, 2006), LaFeAsO (Kamihara *et al.*, 2008) and its derivatives (*cf.* Hunte *et al.*, 2008; Watanabe *et al.*, 2007),

which crystallize in the ZrCuSiAs type (Johnson & Jeitschko, 1974). Contrary to the $HfCuSi_2$ type, Zr is shifted towards Si resulting in the formation of an additional PbO-like layer.

Owing to local *Peierls*-like distortions in the planar layers of arsenic atoms in the $LnTAs_2$ compounds, these atoms have been found to be symmetry breaking, and their positions cannot be described by tetragonal symmetry (Mozharivskiy *et al.*, 2000, 2001; Demchyna *et al.*, 2004). Consequently a reduction in symmetry is necessary. The majority of the $LnAgAs_2$ and $LnAuAs_2$ compounds have been found to crystallize as commensurate superstructures of the $HfCuSi_2$ type in one of the orthorhombic space groups *Pmcn* (No. 62) or *Pcmb* (No. 57). The compounds crystallizing in the space group *Pmcn* are twofold superstructures with lattice parameters a_0, b_0, $2c_0$ with respect to the $HfCuSi_2$ type; the distorted structure contains zigzag chains of the As atoms in the planar layer. The compounds crystallizing in space group *Pcmb* are fourfold superstructures with lattice parameters $\sqrt{2}a_0$, $\sqrt{2}b_0$, $2c_0$ and comprise *cis–trans* chains of the As atoms of the planar layer (Eschen & Jeitschko, 2003; Demchyna *et al.*, 2004). The atomic positions of the superstructures can be deduced from those of the parent structure (aristotype) by group–subgroup relations (Bärnighausen, 1980; Wondratschek & Müller, 2006).

During recent investigations of single crystals of $CeAu_{1-\delta}As_2$ satellite reflections indicating an incommensurate modulation have been observed. The structure model developed for this compound is presented in the following.

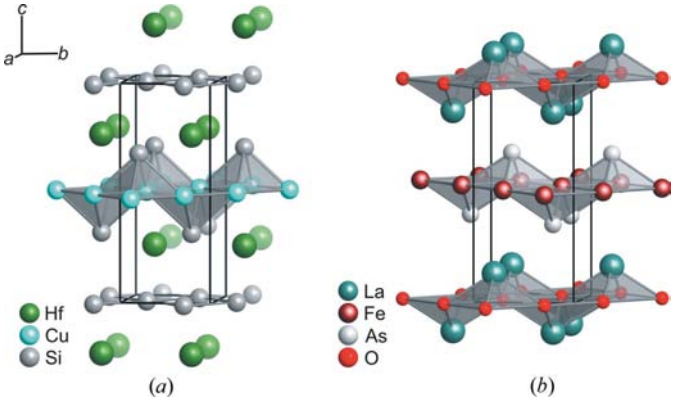

Figure 1
Structural relationship of (*a*) the $HfCuSi_2$ type and (*b*) LaFeAsO (both in *P*4/*nmm*, No. 129).

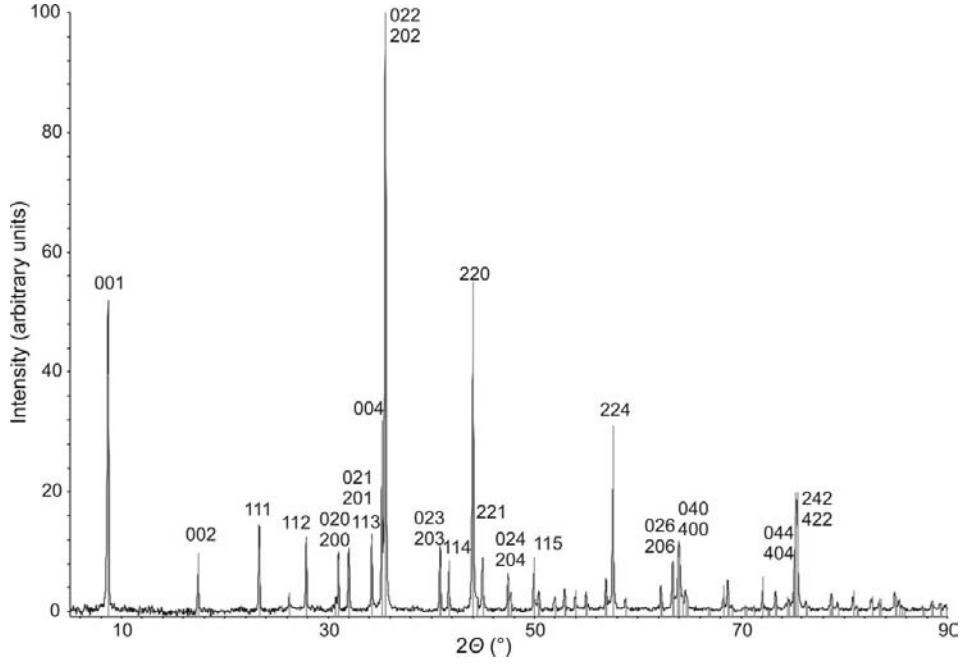

Figure 2
X-ray powder diffraction pattern of $CeAu_{1-\delta}As_2$ and calculated pattern according to the basic structure in space group $P12_1/m1$ (No. 11).

2. Experimental

2.1. Synthesis

The preparation was carried out in an argon-filled glove box [M. Braun, $p(O_2) \leq 1$ p.p.m., $p(H_2O) \leq 1$p.p.m., argon purification with molecular sieve and copper catalyst] in order to avoid reaction of the elements with air and moisture. Pieces of cerium freshly filed from rods (99.9% metal based, TBL Kelpin), gold (powder, 99.9+%, Chempur GmbH) and arsenic (powder, > 99.997% metal based, Aldrich; As_2O_3 removed by sublimation prior to use) were mixed in the atomic ratio of 1:1:2. The reaction was carried out in a sixfold excess of a LiCl/KCl flux (LiCl, KCl: powders, p.a, Merck, dried at 413 K in dynamic vacuum prior to use) in glassy carbon crucibles, which were sealed in evacuated silica tubes. The samples were heated up to 1123 K for 48 h, annealed for 96 h, and cooled to 623 K over 192 h. The flux was removed with water and the products were washed with ethanol. Air-stable, shiny black platelets of the title compound were obtained.

2.2. X-ray investigations

Powder samples of the reaction products were measured on a Stadi P diffractometer (Stoe & Cie GmbH, Cu $K\alpha_1$, Ge monochromator) and the data was analyzed with the *WinXPow* program package (Stoe & Cie, 1999*a*). Buerger precession photographs (Zr-filtered Mo radiation, imaging-plate system) were taken in order to check the quality of the crystals and to determine the lattice parameters and the reflection conditions. A dataset was recorded on an

Table 1
Wyckoff positions, atomic coordinates, isotropic displacement parameters (Å^2) and Fourier coefficients of the modulation wavefunctions of $CeAu_{1-\delta}As_2$ in superspace group $P12_1/m1(\alpha 0\gamma)00$.

Fourier coefficients x, y, z correspond to the atomic displacement wave, o to the occupancy modulation wavefunctions.

Atom	Wyckoff position	x	y	z	U_{iso}
Ce1	2*e*	0.0005 (4)	1/4	0.23003 (4)	0.0126 (1)
Ce2	2*e*	0.5001 (4)	3/4	0.24019 (4)	0.0122 (1)
Au	4*f*	0.24822 (4)	−0.0005 (2)	0.4993 (1)	0.0187 (1)
As1	2*e*	0.9978 (6)	1/4	0.6804 (1)	0.0142 (2)
As2	2*e*	0.4991 (6)	3/4	0.6781 (1)	0.0141 (2)
As3	4*f*	0.2790 (1)	−0.0038 (6)	0.0001 (3)	0.0208 (2)

Atom	$x$sin 1	$y$sin 1	$z$sin 1	$x$cos 1	$y$cos 1	$z$cos 1
Ce1	0.0044 (3)	0	−0.0012 (2)	0.0039 (3)	0	0.0005 (2)
Ce2	0.0067 (3)	0	0.0000 (2)	0.0043 (3)	0	−0.0011 (2)
Au	0.0074 (1)	−0.0011 (2)	0.0002 (1)	0.0001 (3)	0.0001 (1)	0.0004 (1)
As1	0.0062 (4)	0	−0.0022 (4)	−0.0030 (4)	0	0.0011 (4)
As2	0.0056 (4)	0	−0.0015 (4)	−0.0028 (4)	0	0.0006 (4)
As3	0.0052 (3)	−0.005 (5)	0.0006(2)	−0.0037 (7)	−0.0141 (2)	0.0010 (3)

Au	o	$o$sin 1	$o$cos 1
	0.986 (2)	−0.057 (4)	−0.008 (7)

imaging-plate diffraction system (IPDS II, Stoe & Cie, Mo $K\alpha$ radiation, graphite monochromator). The description of the habitus of the platelet was optimized using sets of symmetrically equivalent reflections (*XShape*/*XRed*32, Stoe & Cie, 1999*b*, 2001). A numerical absorption correction was applied using the *JANA*2000 software package (Petříček *et al.*, 2000) and the structure model was refined with *JANA*2000.

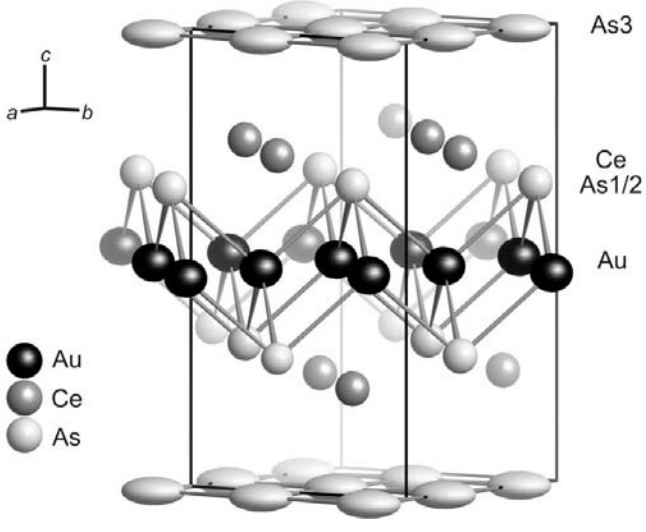

Figure 3
Basic structure for $CeAu_{1-\delta}As_2$ in $P12_1/m1$ (No. 11), ellipsoids at the 99% probability level.

3. Discussion

3.1. Powder samples

The X-ray powder diffraction pattern of $CeAu_{1-\delta}As_2$ is shown in Fig. 2. The lines represent the calculated peaks based on the three-dimensional basic structure model in space group $P12_1/m1$ (No. 11), which has been deduced as the basic space group and will be illustrated in the discussion of the modulated structure. No additional diffraction maxima that could be attributed to by-products were detected. A careful examination shows a broadening of some reflections at higher 2θ values, *e.g.* reflections 242 and 422 at $2\theta \simeq 75^\circ$. This is a strong indication for an orthorhombic distortion of the tetragonal cell of the aristotype at least. The lattice parameters at 293 (2) K have been determined as a = 5.804 (1), b = 5.814 (1) and c = 10.179 (1) Å from powder data.

3.2. Basic structure

Precession photographs of $CeAu_{1-\delta}As_2$ reveal a (pseudo-)tetragonal unit cell with $a \simeq b \simeq 5.8$ Å and $c \simeq 10$ Å. The satellite reflections are visible as blurred spots only. From diffractometer data collection at T = 293 K, lattice parameters of a = 5.803 (1), b = 5.813 (1), c = 10.179 (1) Å and β = 90.09 (8)° are obtained which are in good agreement with those determined from powder data. According to symmetry and reflection conditions (*see below*) the monoclinic space group $P12_1/m1$ (No. 11) was chosen for the basic structure. A structure model of the basic structure was developed confirming the close relationship to the $HfCuSi_2$ type. PbO-like layers consisting of square nets of the Au atoms, alternately capped by As1 and As2 atoms, as well as planar square nets of As3 atoms are stacked along [001]. The Ce atoms occupy positions between these two building blocks. The basic structure of $CeAu_{1-\delta}As_2$ is shown in Fig. 3.

Each Ce atom is surrounded by a square antiprism of As1 and As2 atoms of the PbO-like layer and As3 atoms of the

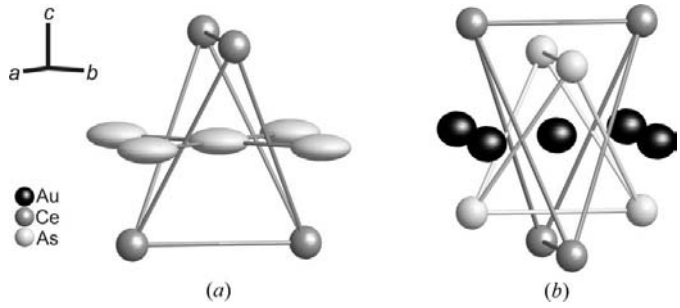

Figure 4
Coordination polyhedra for (*a*) the As3 atom and (*b*) the Au atom in $P12_1/m1$, ellipsoids at the 99% probability level.

square nets leading to three different Ce—As distances. The As1 and As2 atoms are surrounded by a square antiprism of Ce and Au atoms, the As3 atoms by four As3 atoms and four Ce atoms. The latter motif can be described as a (4 + 4) coordination, set up by a compressed tetrahedron of Ce atoms and a rectangle of As3 atoms around the central As3 atom (Fig. 4*a*). A (4 + 4 + 4) coordination is realised for the Au atoms consisting of two interpenetrating elongated tetrahedra of Ce or As1 and As2 atoms, and a rectangle with nearly equal sides of Au atoms (Fig. 4*b*). The Wyckoff positions, atomic coordinates and displacement parameters of the basic structure of $CeAu_{1-\delta}As_2$ are summarized in Table 1. The quite large anisotropic displacement parameters of the As3 atoms can be taken as a hint of the modulation.

3.3. Modulated structure

Reciprocal lattice layers, reconstructed from the diffractometer datasets, show satellites of low intensities in reciprocal layers $l \pm 0.39$. Owing to the position of the additional reflections and a constant splitting of their intensity maxima (*cf.* Fig. 5), commensurate superstructures and twinning of three-dimensional structures can be excluded as reasons for the additional reflections. In fact, we deal here with an incommensurate modulation.

Analysis of the fractional indices of the satellite reflections reveal that they can be indexed with four integer indices *hklm* according to

$$\mathbf{H}_i = h\mathbf{a}_1 * + k\mathbf{a}_2 * + l\mathbf{a}_3 * + m\mathbf{q}, \quad (1)$$

with

$$\mathbf{q} = \alpha\mathbf{a} * + \beta\mathbf{b} * + \gamma\mathbf{c} * . \quad (2)$$

The structure was thus treated as a one-dimensional modulated structure employing the superspace formalism (see below; de Wolff *et al.*, 1981; van Smaalen, 1995, 2007). Atomic positions are described as the sum of the average positions and the modulation wavefunctions. The latter are given as a truncated Fourier series, where the Fourier coefficients are used as independent parameters in the refinement

$$u_i(\overline{x}_{s_4}) = \sum_{n_1=0}^{\infty} A_i^{n_1} \cos(2\pi n_1 \overline{x}_{s_4}) + B_i^{n_1} \sin(2\pi n_1 \overline{x}_{s_4}), \quad (3)$$

where i = 1, 2, 3 or (x, y, z) and $A_i^{n_1}$ and $B_i^{n_1}$ are the structural parameters. The fourth superspace coordinate is defined by

$$\overline{x}_{s_4} = t - \mathbf{q} \cdot \mathbf{r}_0, \quad (4)$$

with $\mathbf{r}^0$ denoting the average position of the atoms and t defining the section of superspace or the initial phase of the modulation functions. Similar modulation functions were used for the anisotropic displacement parameters.

A section of the reciprocal layer *h2l*, recalculated from the recorded dataset, is shown in Fig. 5(*a*). Looking at the area around the main reflection 421, *e.g.* two of the satellites can be

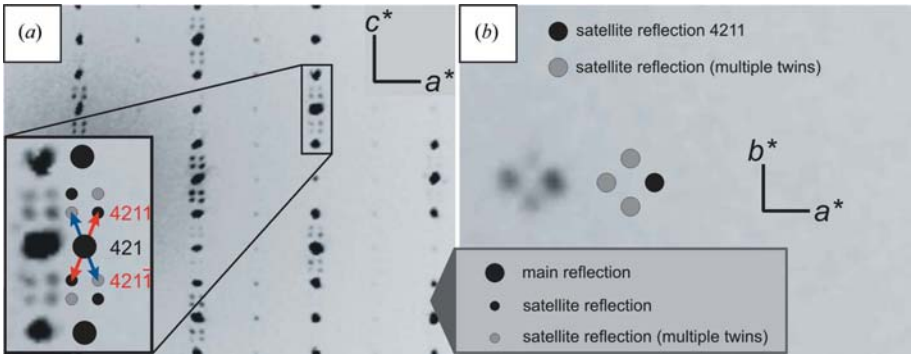

Figure 5
Satellite pattern in the diffraction image of $CeAu_{1-\delta}As_2$, (*a*) area around main reflection 421 (section of the reciprocal layer *h2l*) and (*b*) satellite reflection 4211 with contribution of twin individuals in a section of the reciprocal layer *hk*1.39.

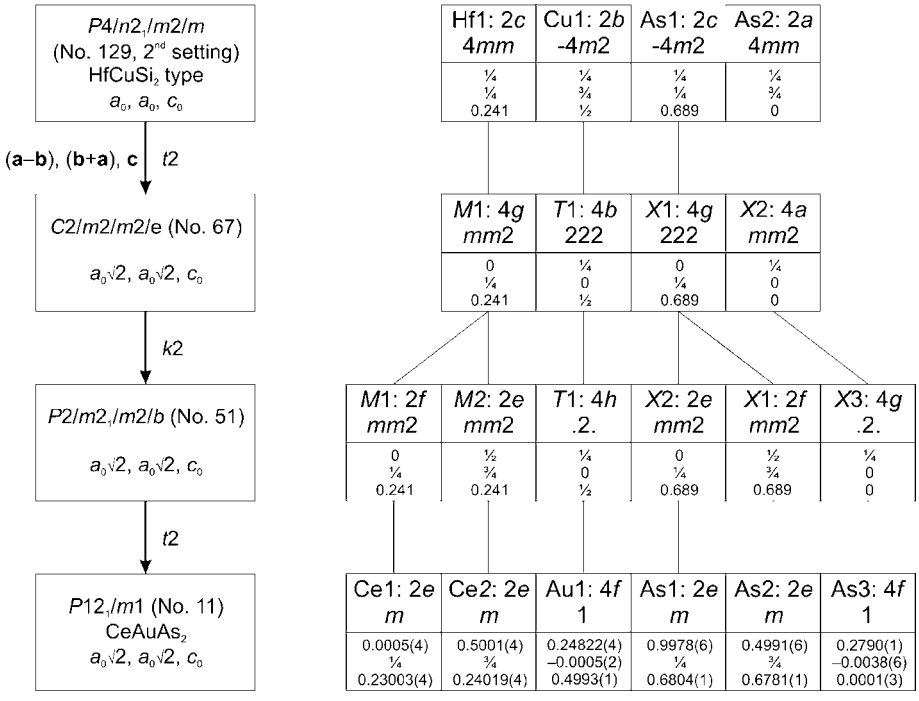

Figure 6
Bärnighausen tree for the symmetry relation between the $HfCuSi_2$ (*P4/nmm*) and the $CeAu_{1-\delta}As_2$ structure ($P12_1/m1$). Note that the atomic positions of the $HfCuSi_2$ type are shifted by $z + \frac{1}{2}$ with respect to the data given in the original publication (Andrukhiv *et al.*, 1975).

Table 2
Crystallographic and refinement data for $CeAu_{1-\delta}As_2$.

Chemical formula	$CeAu_{0.986\,(2)}As_2$†
M_r	484.18
Crystal system, superspace group	Monoclinic, $P12_1/m1(\alpha0\gamma)00$ (No. 11.1)
Temperature (K)	293
a, b, c (Å)	5.804 (1), 5.814 (1), 10.179 (1)
β (°)	90.09 (8)
V (Å^3)	343.48 (9)
Modulation wavevector	$\mathbf{q} = \alpha\mathbf{a}^* + \beta\mathbf{b}^* + \gamma\mathbf{c}^*$
Wavevector component	$\alpha = 0.08$ (1), $\beta = 0$, $\gamma = 0.39$ (1)
Z	4
Radiation type	Mo $K\alpha$
μ (mm^{-1})	74.55
Crystal form, size (mm)	Platelet, 0.139 × 0.137 × 0.004
Data collection	
Diffractometer	Stoe IPDS II, graphite monochromator
Sample detector distance (mm)	70
Data collection method	ω scans
Absorption correction	Numerical
T_{min}, T_{max}	0.015, 0.306
No. of measured, independent and observed reflections	20919, 4210, 1422
Criterion for observed reflections	$I > 3\sigma(I)$
No. of unique reflections (all/obs)	4210, 1422
No. of main reflections (all/obs)	1342, 1044
No. of satellite reflections (all/obs)	2868, 378
R_{int}, R_σ	0.0681, 0.0190
θ_{max} (°)	33.5
Refinement	
Refinement on	F
Refined modulation wave	$1\cdot\mathbf{q}$
R_1, wR_2 ($I > 3\sigma$); R_1, wR_2 (overall)	0.0342, 0.0364; 0.0984, 0.0395
R_1, wR_2 ($I > 3\sigma$); R_1, wR_2 (all I) (main reflections)	0.0292, 0.0319; 0.0380, 0.0326
R_1, wR_2 ($I > 3\sigma$); R_1, wR_2, (all I) (satellites)	0.0919, 0.0922; 0.3728, 0.1119
S (all I)	1.25
No. of reflections	4210
No. of parameters	134
$(\Delta/\sigma)_{max}$	0.041
$\Delta\rho_{max}$, $\Delta\rho_{min}$ (e Å^{-3})	2.49, −2.29
Extinction method	Becker & Coppens (1974)
Extinction coefficient	0.53 (2)
Twin laws	$\begin{vmatrix}1&0&0\\0&1&0\\0&0&1\end{vmatrix}$ $\begin{vmatrix}0&\bar1&0\\1&0&0\\0&0&1\end{vmatrix}$ $\begin{vmatrix}\bar1&0&0\\0&\bar1&0\\0&0&1\end{vmatrix}$ $\begin{vmatrix}0&1&0\\\bar1&0&0\\0&0&1\end{vmatrix}$
Twin volume fractions	0.009 (9), 0.451 (6), 0.072 (3), 0.467 (6)

† Three decimal points for the composition of $CeAu_{0.986\,(2)}As_2$ were chosen to emphasize the deviation from the ideal 1:1:2 composition.

attributed to the modulation vector $\mathbf{q}$ and $-\mathbf{q}$, respectively. The components of $\mathbf{q}$ were refined to $\alpha = 0.08$ (1), $\beta = 0.00$ (1) and $\gamma = 0.39$ (1) without symmetry constraints (*X-Area*, 2006). These satellites, 4211 and $42\bar{1}\bar{1}$, are marked by red arrows. Obviously, two further satellites, indicated by blue arrows, are found around the main reflection 421, which can either be the result of a second modulation vector or of twinning of the crystal. As no cross terms, *i.e.* satellites attributed to the modulation vectors $\mathbf{q}_1 + \mathbf{q}_2$ and $\mathbf{q}_1 - \mathbf{q}_2$ with $\mathbf{q}_1 = (\alpha0\gamma)$ and $\mathbf{q}_2 = (-\alpha0\gamma)$, were detected a two-dimensional modulation can be excluded. Moreover, the section of the reciprocal layer $hk1.39$, depicted in Fig. 5(*b*), shows a pattern of four satellite maxima, one being 4211 again (emphasized by a black dot in the figure). This satellite pattern can only be the result of multiple twinning owing to the stepwise loss of symmetry in accordance with the *Bärnighausen* tree stated in Fig. 6 (*see below*). As can also be seen from Fig. 5, some of the main reflections show anomalies, like a tendency to splitting or streaking. This can also be taken as evidence for twinning. The structure has hence been refined as a fourfold twin.

Since the modulation wavevector $\mathbf{q} = 0.08\,(1)\mathbf{a}^* + 0.39\,(1)\mathbf{c}^*$ is incompatible with tetragonal or orthorhombic symmetry, the symmetry has to be reduced to the monoclinic crystal system. Owing to the reflection conditions for the satellites, the monoclinic superspace group $P12_1/m1(\alpha0\gamma)00$ (No. 11.1; Janssen *et al.*, 2004) was chosen. Applying the restrictions for the monoclinic crystal system the lattice parameters were refined to $a = 5.804$ (1), $b = 5.814$ (1), $c = 10.179$ (1) Å and $\beta = 90.09$ (8)°. Based on the parent $HfCuSi_2$-type structure in the space group $P4/nmm$ (No. 129), a three-dimensional model in this superspace group was developed following the *Bärnighausen* formalism stated in Fig. 6 (Bärnighausen, 1980; Wondratschek & Müller, 2006). The reduction in symmetry *via* two *translationengleiche* and one *klassengleiche* steps of index

Table 3
Interatomic distances (Å) in the modulated structure of $CeAu_{1-\delta}As_2$.

	Average	Minimum	Maximum
Ce1—As1^{i}	3.047 (1)	3.042 (1)	3.052 (1)
Ce1—As1^{ii}	3.047 (1)	3.042 (1)	3.052 (1)
Ce1—As2^{iii}	3.048 (5)	3.024 (5)	3.071 (5)
Ce1—As2^{ii}	3.050 (5)	3.040 (5)	3.060 (5)
Ce1—As3	3.207 (4)	3.177 (5)	3.237 (5)
Ce1—As3^{iv}	3.187 (4)	3.159 (5)	3.217 (5)
Ce1—As3^{v}	3.187 (4)	3.159 (5)	3.217 (5)
Ce1—As3^{vi}	3.207 (4)	3.177 (5)	3.237 (5)
Ce2—As1^{ii}	3.002 (5)	2.974 (5)	3.029 (5)
Ce2—As1^{vii}	3.023 (5)	3.012 (5)	3.034 (5)
Ce2—As2^{ii}	3.024 (1)	3.019 (1)	3.029 (1)
Ce2—As2^{viii}	3.024 (1)	3.019 (1)	3.029 (1)
Ce2—As3^{ix}	3.107 (4)	3.065 (5)	3.151 (5)
Ce2—As3^{x}	3.134 (4)	3.080 (5)	3.188 (5)
Ce2—As3^{xi}	3.134 (4)	3.080 (5)	3.188 (5)
Ce2—As3^{vi}	3.107 (4)	3.065 (5)	3.151 (5)
Au1—Au1^{xii}	2.882 (2)	2.870 (3)	2.893 (3)
Au1—Au1^{i}	2.923 (3)	2.913 (3)	2.932 (3)
Au1—Au1^{xiii}	2.901 (2)	2.889 (2)	2.914 (2)
Au1—Au1^{vi}	2.913 (2)	2.900 (2)	2.925 (2)
Au1—As1^{xiv}	2.765 (4)	2.735 (4)	2.795 (4)
Au1—As1^{i}	2.735 (4)	2.718 (4)	2.753 (4)
Au1—As2^{xv}	2.744 (4)	2.720 (4)	2.767 (4)
Au1—As2^{ii}	2.747 (4)	2.719 (4)	2.773 (4)
As3—As3^{iv}	3.241 (5)	3.211 (6)	3.275 (6)
As3—As3^{xvi}	2.569 (5)	2.519 (6)	2.623 (6)
As3—As3^{xii}	2.861 (6)	2.699 (5)	3.026 (5)
As3—As3^{vi}	2.953 (6)	2.788 (5)	3.115 (5)

Symmetry codes: (i) $1-x, -y, 1-z$; (ii) $1-x, 1-y, 1-z$; (iii) $-x, 1-y, 1-z$; (iv) $-x, -y, -z$; (v) $-x, \frac{1}{2}+y, -z$; (vi) $x, \frac{1}{2}-y, z$; (vii) $2-x, 1-y, 1-z$; (viii) $1-x, 2-y, 1-z$; (ix) $x, 1+y, z$; (x) $1-x, 1-y, -z$; (xi) $1-x, \frac{1}{2}+y, -z$; (xii) $-x, -y, 1-z$; (xiii) $x, -\frac{1}{2}-y, z$; (xiv) $-1+x, y, z$; (xv) $x, -1+y, z$; (xvi) $1-x, -y, -z$.

Table 4
Distances (Å) in and between the As3 chains in different blocks.

	Rectangles	Four chains	Five chains	Six chains	Seven chains
a_b	2.557–2.562	2.535–2.545	2.534–2.553	2.582–2.618	2.572–2.620
b_b	2.854–2.895	2.778–2.851	2.779–2.888	2.702–2.855	2.704–2.896
a_{nb}	–(one 'chain')	3.269–3.275	3.264–3.274	3.221–3.232	3.222–3.237
b_{bc}	2.910–2.950	2.953–3.027	2.917–3.026	2.972–3.102	2.909–3.101

a and *b*: crystallographic directions (*b* in propagation direction of the chains); indices: b = bonding, nb = non-bonding, bc = between chains.

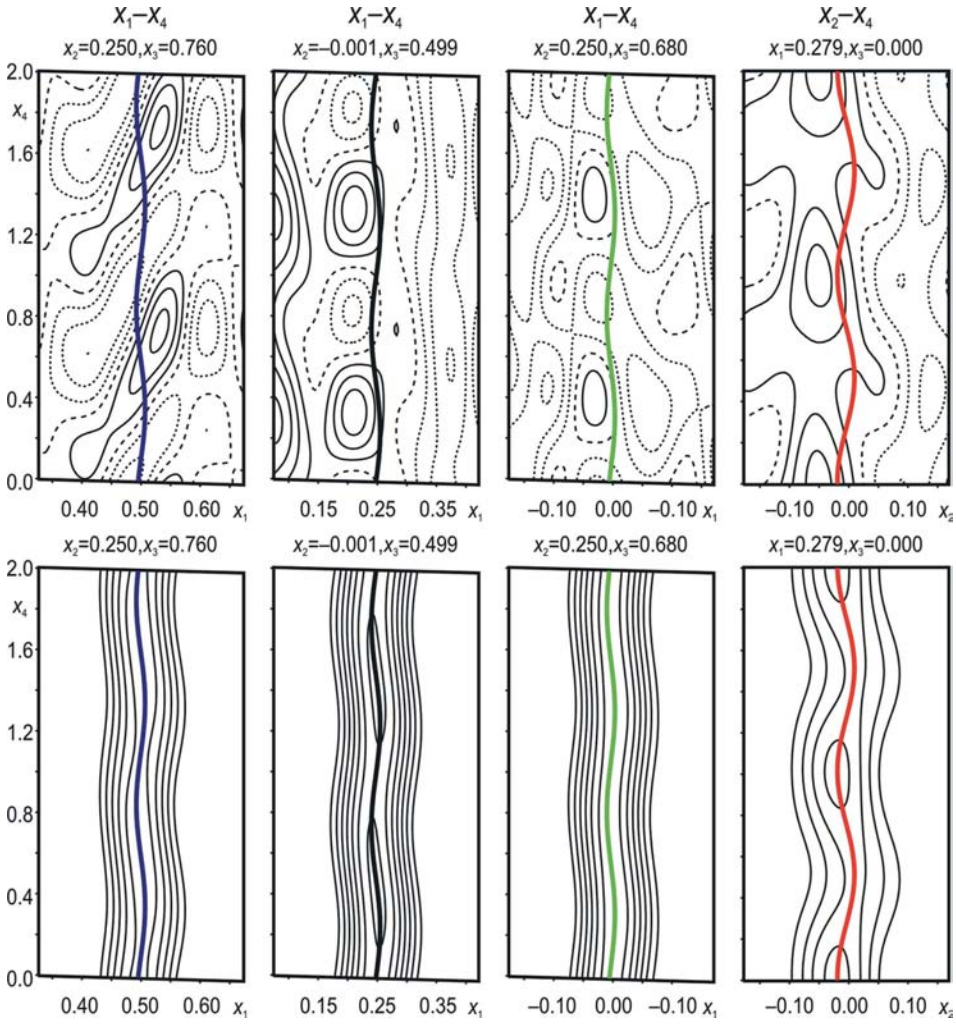

Figure 7
Difference-Fourier maps (top) and Fourier maps (bottom) for Ce1, Au, As1 (all x_1–x_4) and As3 (x_2–x_4), bold lines: calculated atomic modulation functions for Ce1 (blue), Au (black), As1 (green) and As3 (red); steps of electron densities 0.5 e Å^{-3} per line in the difference-Fourier maps and 40 e Å^{-3} per line for Ce, Au, 20 e Å^{-3} per line for As in the Fourier maps. Ce2 and As2 are not shown since they exhibit a similar behavior to Ce1 and As1 (*cf.* Fig. 8).

2 reflects the $\sqrt{2}\cdot\sqrt{2}$ superstructure in the first step, the loss of the *C*-centering in the second, and the removal of mirror planes in the last. Note that the space group and the atom sites of commensurately modulated $CeAgAs_2$ (Demchyna *et al.*, 2004) can be obtained in a similar way. During each of the two *translationengleiche* symmetry-reduction steps twinning is likely to occur and the result is a fourfold twin in the end. The *klassengleiche* step may give rise to the formation of antiphase domains.

In accordance with the results of the commensurate superstructure of $CeAgAs_2$ (Demchyna *et al.*, 2004), the displacement of the As3 atoms was found to be the predominant effect of the modulation. After introduction of one harmonic modulation wave for the positional modulation and the displacement parameters of all atoms (higher modulation waves were not considered as only first-order satellites were observed in the diffraction data), the Fourier maps around the Au atom indicated a slight modulation of the electron-density distribution for this site as well. Consequently, a harmonic occupancy modulation wave was introduced for the Au atom, which led to a considerable drop in the *R* values. The Au occupancy was refined to 0.985 (2). Transition metal deficiency in $HfCuSi_2$-related structures has also been found for some antimonides (Cordier *et al.*, 1985; Ferguson *et al.*, 1996). No occupancy modulations have been observed for the Ce and As atoms. The atomic parameters are listed in Table 1, final results of the refinements as well as relevant crystallographic data can be found in Table 2,[1] interatomic distances are shown in Table 3 and distances in and between the As3 chains are listed in Table 4.

The refined atomic modulation functions are displayed embedded in the respective difference-Fourier ($F_o - F_c$) and Fourier (F_o) maps in Fig. 7 (only the direction associated with the largest displacement of each atom has been chosen to exemplify the results of the positional modulation). As can clearly be seen from these maps, the As3 atoms are mainly displaced

[1] Supplementary data for this paper are available from the IUCr electronic archives (Reference: CK5035). Services for accessing these data are described at the back of the journal.

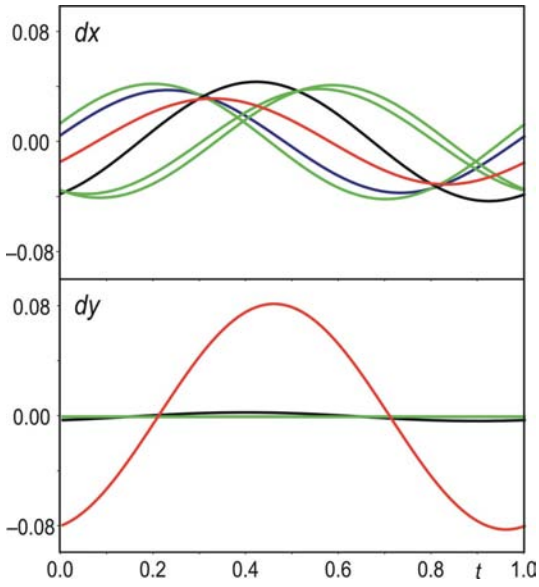

Figure 8
t plots of the positional modulations for $CeAu_{1-\delta}As_2$ (Ce blue lines, Au black line, As1 and As2 green lines, As3 red line) along [100] (*dx*) and [010] (*dy*).

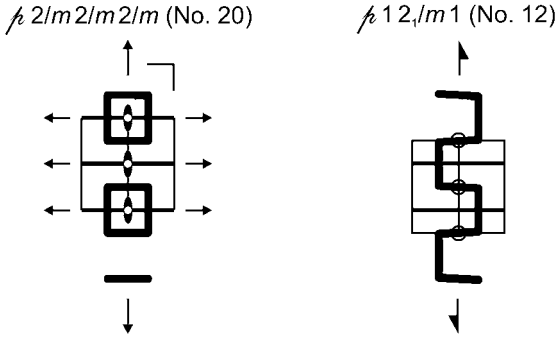

Figure 9
Rod groups of the different motifs (projection along [001]): rectangles in rod group *p*2/*m*2/*m*2/*m* (No. 20, left) and *cis–trans* chains in rod group $p12_1/m1$ (No. 12, right)

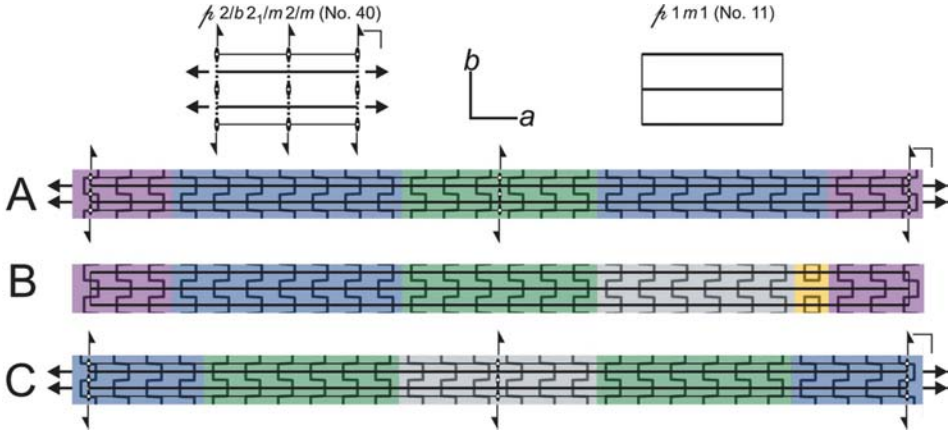

Figure 10
Top: sketches of the different layer groups: left: $p2/b\ 2_1/m\ 2/m$ (No. 40), right: *p*1*m*1 (No. 11). Bottom: layers A, B and C (projection along [001]) – layers A and C possess $p2/b2_1/m2/m$ symmetry, B and $\overline{\text{B}}$ (not shown; inverse sequence along **a**) *p*1*m*1 symmetry.

in the [010] direction resulting in the formation of *cis–trans* chains with enlarged gaps between the chains. The distortion within the arsenic nets also influences the other atoms, shown in the *t* plots (Fig. 8) for Ce1, Ce2, Au, As1 and As2. The positional modulation of the As3 atoms along x_2 causes a dislocation of the Ce atoms along x_1 and – transferred by the latter – the As1, As2 and Au atoms of the PbO-like layers along x_1 also. The electron-density distribution is modeled well by the calculated atomic modulation functions (lower panel of Fig. 7), the $F_o - F_c$ maps are quite smooth, the largest difference peaks and holes were calculated to 2.5 and -2.3 e Å^{-3}.

As mentioned above, the primary result of the modulation is the formation of *cis–trans* chains of As3 atoms running along [010]. The As3—As3 intra-chain distances change from $\sim$2.519 (1) to 2.621 (1) Å along [100], and 2.700 (2) to 2.906 (2) Å along [010] as a result of the positional modulation. Choosing 2.907 Å as the upper limit for bonded As3 atoms, three different motifs can be identified: *cis–trans* chains in *in-phase* or in *anti-phase* orientations (*in-phase* orientation is defined as the orientation of the chains of the majority case), and As_4 rectangles on the border between *in-phase* and *anti-phase* chains. The rod groups of these motifs were determined according to *International Tables for Crystallography* (Kopsky & Litvin, 2006). The propagation direction of the *cis–trans* chains and consequently the long edges of the rectangles are along [010]. The chains comprise monoclinic/rectangular $p12_1/m1$ (No. 12) symmetry, whereas the rectangles possess orthorhombic *p*2/*m*2/*m*2/*m* (No. 20) symmetry, *cf.* Fig. 9.

The *cis–trans* chains are grouped in blocks of different length, depicted in Fig. 10. Blocks consisting of seven (blue) or six (grey) chains in the *in-phase* orientation, and six (green) or five (red) chains in the *anti-phase* orientation are found. The modulation of the As3—As3 intra-chain distances also causes a sudden change between the majority and the minority blocks at the border of the blocks. As explained above, the direct *in-phase–anti-phase* change is mediated in some cases by a row of rectangles of As3 atoms. The sequence of these blocks in an extended section of the modulated As net results in a complicated pattern of four different arrangements along [100]. These arrangements, hereafter denoted as layers A, B, $\overline{\text{B}}$ and C cover 25 basic unit each, Fig. 10. Since layer $\overline{\text{B}}$ reveals the same sequence but the inverse order of B, only layer B is shown in the figure. The centrosymmetric layers A and C exhibit orthorhombic layer group symmetry $p2_1/m2/a2/m$ (No. 40), whereas the noncentrosymmetric layers B and $\overline{\text{B}}$ reveal monoclinic/rectangular symmetry *p*1*m*1 (No. 11). The stacking sequence of the layers along [001] results

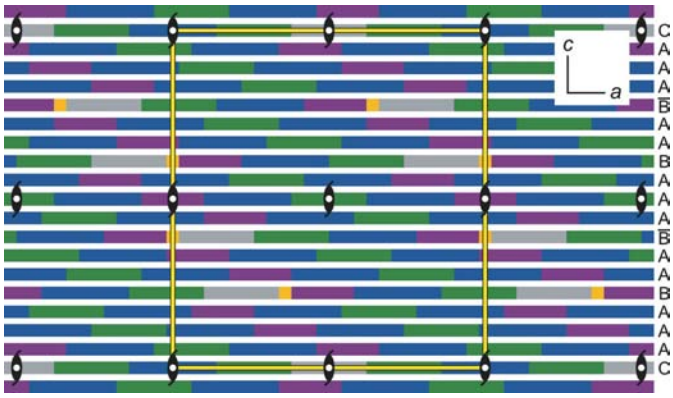

Figure 11
Stacking of layers A, B, $\overline{\text{B}}$ and C along [010]. The yellow rectangle indicates a monoclinic repetition unit compatible with which spreads over $25 \times 1 \times 18$ basic unit cells and contains 13 layers A, two layers B, two layers $\overline{\text{B}}$ and one layer C stacked in the sequence CAAABAA$\overline{\text{B}}$AAABAA$\overline{\text{B}}$AAA. The screw axes and centers of symmetry of space group $P12_1/m1$ are emphasized.

in the pattern displayed in Fig. 11. As indicated in Fig. 11, the stacking is compatible with monoclinic symmetry $P12_1/m1$ and a repetition unit of $25 \times 1 \times 18$ basic unit cells ($a' = 25\,a$, $b' = 1b$, $c' = 18c$ and $\beta' = \beta$), emphasized by the yellow rectangle, can be designated. Note that only the As net is discussed here and that this repetition unit is not an approximant of the entire modulated structure. This repetition unit consists of 13 layers A, two layers B, two layers $\overline{\text{B}}$ and one layer C, which are arranged in the sequence CAAABAA$\overline{\text{B}}$AAABAA$\overline{\text{B}}$AAA. The different layers are shifted along [100] for either $-5a_0$ or $+8a_0$. The number of *anti-phase* chains in the minority blocks of the repetition unit divided by the number of *in-phase* chains tends to the value of 0.39 and hence reflects the value of γ of the modulation vector.

Financial support by the Deutsche Forschungsgemeinschaft (Sonderforschungsbereich 463) is gratefully acknowledged.

References

Andrukhiv, L. S., Lysenko, L. A., Yarmolyuk, Ya. P. & Gladyshevskii, E. I. (1975). *Dopov. Akad. Nauk Ukr. RSR Ser. A*, pp. 645–648.
Bärnighausen, H. (1980). *Match*, **9**, 139–175.
Becker, P. J. & Coppens, P. (1974). *Acta Cryst.* A**30**, 129–147.
Brechtel, E., Cordier, G. & Schäfer, H. (1979). *Z. Naturforsch. B*, **35**, 1–3.
Brylak, M., Möller, M. H. & Jeitschko, W. (1995). *J. Solid State Chem.* **115**, 305–308.
Chykhrij, S. I., Loukasouk, G. V., Oryshchyn, S. V. & Kuz'ma, Yu. (1997). *J. Alloys Compd.* **248**, 224–232.
Cordier, G., Schäfer, H. & Woll, P. (1985). *Z. Naturforsch. B*, **40**, 1097–1099.
Demchyna, R., Jemetio, J. P. F., Prots, Yu., Doert, Th., Akselrud, L. G., Schnelle, W., Kuz'ma, Yu. B. & Grin, Yu. (2004). *Z. Anorg. Allg. Chem.* **630**, 635–641.
Demchyna, R. O., Kuz'ma, Yu. B. & Babizhetsky, V. S. (2001). *J. Alloys Compd.* **315**, 158–163.
Eisenmann, B., May, N., Müller, W. & Schäfer, H. (1972). *Z. Naturforsch. B*, **27**, 1155–1157.
Eisenmann, B., May, N., Müller, W., Schäfer, H., Weiss, A., Winter, J. & Ziegleder, G. (1970). *Z. Naturforsch.* **25**, 1350–1352.
Eschen, M. & Jeitschko, W. (2003). *Z. Naturforsch. B*, **58**, 399–409.
Ferguson, M. J., Hushagen, R. W. & Mar, A. (1996). *Inorg. Chem.* **35**, 4505–4512.
Hunte, F., Jaroszynski, J., Gurevich, A., Larbalestier, D. C., Jin, R., Sefat, A. S., McGuire, M. A., Sales, B. C., Christen, D. K. & Mandrus, D. (2008). *ArXiv.Org, e-Print Archive, Condens. Matter*, 0804.0485.
Janssen, T., Janner, A., Looijenga-Vos, A., de Wolff, P. M. & Prince, E. (2004). *International Tables for Crystallography*, Vol. C, ch. 9.8. Dordrecht: Kluwer Academic Publishers.
Jemetio, J. P., Doert, Th. & Böttcher, P. (2002). *Z. Kristallogr. New Cryst. Struct.* **217**, 455–457.
Jemetio, J. P., Doert, Th., Rademacher, O. & Böttcher, P. (2002). *J. Alloys Compd.* **338**, 93–98.
Johnson, V. & Jeitschko, W. (1974). *J. Solid State Chem.* **11**, 161–166.
Kamihara, Y., Hiramatsu, H., Hirano, M., Kawamura, R., Yanagi, H., Kamiya, T. & Hosono, H. (2006). *J. Am. Chem. Soc.* **128**, 10012–10013.
Kamihara, Y., Watanabe, T., Hirano, M. & Hosono, H. (2008). *J. Am. Chem. Soc.* **130**, 3296–3297.
Kolenda, M., Oles, A. & Szytula, A. (2001). *J. Alloys Compd.* **322**, 55–58.
Kopsky, V. & Litvin, D. B. (2006). Editors. *International Tables for Crystallography*, Vol. E, *Subperiodic groups*, 1st online ed. Chester: International Union of Crystallography [doi:10.1107/97809553502060000105].
Mozharivskiy, Yu., Kaczorowski, D. & Franzen, H. F. (2000). *J. Solid State Chem.* **155**, 259–272.
Mozharivskiy, Yu., Kaczorowski, D. & Franzen, H. F. (2001). *Z. Anorg. Allg. Chem.* **627**, 2163–2172.
Mozharivskiy, Yu., Pecharsky, V. K. & Franzen, H. F. (2002). *J. Alloys Compd.* **345**, 100–104.
Petříček, V., Dušek, N. & Palatinus, L. (2000). *JANA*2000. Institute of Physics, Prague, Czech Republic.
Smaalen, S. van (1995). *Crystallogr. Rev.* **4**, 79–202.
Smaalen, S. van (2007). *Incommensurate Crystallography*. Oxford University Press.
Sologub, O., Hiebl, K., Rogl, P., Noël, H. & Bodak, O. I. (1994). *J. Alloys. Comput.* **210**, 153–157.
Sologub, O., Noël, K., Leithe-Jasper, A., Rogl, P. & Bodak, O. I. (1995). *J. Solid State Chem.* **115**, 441–446.
Stoe & Cie (1999*a*). *WinXPow*. Stoe & Cie, GmbH, Darmstadt, Germany.
Stoe & Cie (1999*b*). *X-Shape*. Stoe & Cie. GmbH, Darmstadt, Germany.
Stoe & Cie (2001). *X-Red*32. Stoe & Cie. GmbH, Darmstadt, Germany.
Stoe & Cie (2006). *X-Area*. Stoe & Cie. GmbH, Darmstadt, Germany.
Venturini, G., Malaman, B. & Roques, B. (1989*a*). *J. Solid State Chem.* **79**, 126–135.
Venturini, G., Malaman, B. & Roques, B. (1989*b*). *J. Solid State Chem.* **79**, 136–145.
Wang, M., McDonald, R. & Mar, A. (1999). *J. Solid State Chem.* **147**, 140–145.
Watanabe, T., Yanagi, H., Kamiya, T., Kamihara, Y., Hiramatsu, H., Hirano, M. & Hosono, H. (2007). *Inorg. Chem.* **46**, 7719–7721.
Wolff, P. M. de, Janssen, T. & Janner, A. (1981). *Acta Cryst.* A**37**, 625–636.
Wondratschek, H. & Müller, U. (2006). Editors. *International Tables for Crystallography*, Vol. A1, 1st. ed. Dordrecht: Kluwer Academic Publishers.
Zheng, C. & Hoffmann, R. (1986). *J. Am. Chem. Soc.* **108**, 3078–3088.